Chemical Science

ROYAL SOCIETY OF CHEMISTRY

EDGE ARTICLE

View Article Online
View Journal | View Issue

Cite this: *Chem. Sci.*, 2024, **15**, 14872

All publication charges for this article have been paid for by the Royal Society of Chemistry

Received 29th June 2024
Accepted 8th August 2024

DOI: 10.1039/d4sc04295f

rsc.li/chemical-science

A redox-active organic cage as a cathode material with improved electrochemical performance†

Saibal Bera,[a] Nicolas Goujon,[a] Manuel Melle-Franco,[b] David Mecerreyes*[ac] and Aurelio Mateo-Alonso *[ac]

Organic cages offer numerous opportunities for creating novel materials suitable for a wide range of applications. Among these, energy-related applications are beginning to attract attention. We report here the synthesis of a [3 + 6] trigonal prismatic cage constituted by three redox-active dibenzotetraazahexacene subunits. Cathodes formulated with the organic cage show enhanced performance compared to those formulated with the individual subunits, showing improvements in terms of electrochemical stability, lithium-ion diffusivity, and cathode capacity.

Introduction

Organic cages (OCs) are discrete polyhedric molecular structures constituted by a rigid framework of covalently linked monomeric subunits that act as nodes and linkers. Such framework generates a well-defined internal cavity and windows of different shapes and dimensions that allow the diffusion of other species in and out of the cavity. Different types of OCs, each with varying stoichiometries and windows of diverse shapes and sizes, can be designed to control the diffusion of various species within the framework.[1–5] This modularity also allows the introduction of monomers with different optical or electronic properties that can be translated to the cage. In contrast to extended porous frameworks, such as metal–organic frameworks, covalent organic frameworks and porous organic polymers, OCs are synthesized and characterized as other organic molecules, which makes their characterization easier by common NMR and MS techniques. In addition, OCs can be dispersed and processed in solution. Furthermore, increasingly complex OCs can be obtained using dynamic covalent chemistry that simplifies their synthesis. Owing to these unique features, OCs present many opportunities as functional materials and their potential has been demonstrated for several applications including encapsulation,[2,6,7] separation,[8–11] molecular reaction vessels,[12–14] and porous liquids,[15] among others; among which, energy related applications are starting to attract attention.[16–21]

In recent years, the development of organic electrode materials for lithium-ion batteries has received significant attention in view of their sustainable and low-cost production, and their low environmental impact.[22–29] Furthermore, the tunability of organic molecules provide unique opportunities to design new electrode materials with optimal properties. Yet, organic electrodes face multiple challenges that are difficult to address since different parameters, such as power density, energy density, ion diffusivity, cycling stability, gravimetric density, conductivity, production costs and recyclability have to be considered. For example, low molecular weight molecules with high capacity can leach into the electrolyte, which limits their cycling stability. Moreover, ion diffusivity is constrained by factors such as the electrode density, the degree of swelling of the electrode in the presence of the electrolyte, and the size of the redox species. Collectively, these factors impose limitations on a battery's capacity to fast charge and discharge effectively. Therefore, the systematic investigation of different classes of materials is crucial for the development of high-performance organic electrodes. An important aspect to enable such fundamental investigations is the synthetic accessibility and availability (multigram scale) of materials at the early research stages.

In this regard, OCs can meet many of the criteria for developing electrode materials for lithium-ion batteries. In principle, they can be engineered to exhibit high specific capacities by the introduction of redox modules, and an efficient diffusion of lithium ions by a careful design of the framework. Furthermore, the synthesis of OCs, once developed, often involves one-step procedures from the monomers that can be potentially scaled up. However, despite their potential, there is only one example where OCs have been used as an organic cathode in lithium-ion batteries to the best of our knowledge,[18] and most importantly, the influence of OCs in electrode performance continues to remain unclear. Herein, we demonstrate that the assembly of organic redox units in a cage-like structure generate materials

[a]*POLYMAT, University of the Basque Country UPV/EHU, Avenida de Tolosa 72, 20018 Donostia-San Sebastián, Spain. E-mail: amateo@polymat.eu; david.mecerreyes@ehu.es*

[b]*CICECO, Aveiro Institute of Materials, Department of Chemistry, University of Aveiro, 3810-193 Aveiro, Portugal*

[c]*Ikerbasque, Basque Foundation for Science, 48009 Bilbao, Spain*

† Electronic supplementary information (ESI) available. See DOI: https://doi.org/10.1039/d4sc04295f

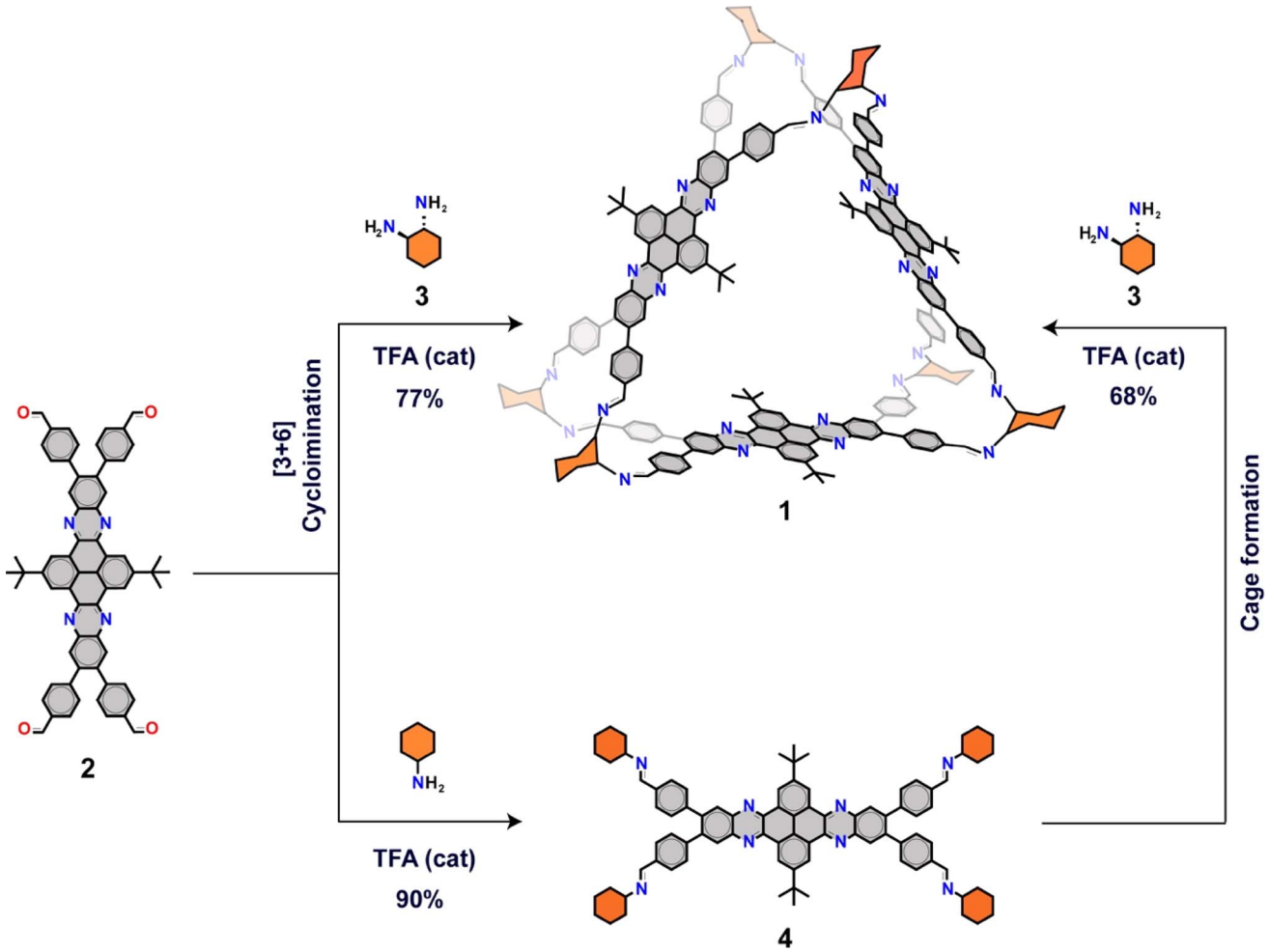

Fig. 1 General route for the synthesis of cage **1** and reference **4**.

with a higher electrochemical performance than the individual redox units. To do so, we have synthesized a new [3 + 6] trigonal prismatic cage (**1**) constituted by three redox-active dibenzotetraazahexacene walls. Cage **1** has been synthesized in a gram scale by condensation between a tetratopic aldehyde, dibenzotetraazahexacene **2**, and a ditopic diamine, (1*R*,2*R*)-1,2-diaminocyclohexane (**3**) (Fig. 1). The gram scale availability of cage **1** has enabled the fabrication and characterization of organic electrodes in lithium-ion batteries. Our results show how the electrochemical performance of the cage-based cathodes is superior in terms of electrolytic stability, lithium-ion diffusivity and capacity to that of compound **4**, a model individual subunit that has been synthesised and investigated under the same conditions as a reference material. The enhanced performance of the cage-based electrodes is consistent with the lower solubility of the cage in the electrolyte that results in an enhanced cycling stability, and with an enhanced diffusivity of lithium ions in the organic cage electrodes.

Results and discussion

To construct the cage, we selected dibenzotetrazahexacene derivatives as redox subunits as they are constituted by fused quinoxaline groups, which have shown a lot of promise as organic cathodes, as a result of their redox properties and high stability.[22,30–35] Cage **1** has been synthesized in a gram-scale from dibenzotetrazahexacene tetraaldehyde **2** and diamine **3** (Fig. 1 and Scheme S1†). Tetraaldehyde **2** (ref. 36) is available in a gram-scale in only four steps from commercially available products and has been synthesized following a slightly modified procedure with a higher yield in the last step that increases from 22% to 78% (see ESI† for details procedure), whereas, diamine **3** is commercially available. Imine condensation between tetraaldehyde **2** and diamine **3** in a 1 : 2 equivalent ratio with a catalytic amount of trifluoroacetic acid (TFA) yields the trigonal prismatic [3 + 6] cage **1** in a 77% yield (Fig. 1).

To investigate the impact of the cage-like assembly on the performance of the electrodes, we synthesized an individual dibenzotetraazahexacene redox subunit condensed to four cyclohexylimines (**4**) as a reference material. Reference **4** was synthesized by condensing tetraldehyde **2** with an excess (10 eq.) of cyclohexylamine in chloroform with a catalytic amount of TFA. Notably, we have observed how reference **4** can be converted into cage **1** (68%) by a transimination reaction in the presence of diamine **3**. In addition, when cage **1** was exposed to the same transimination conditions in the presence of

cyclohexylamine, no transformation was observed, indicating that the cage is the most thermodynamically stable product in these conditions.

Cage **1** is sparingly soluble in common organic solvents, among which, the higher solubilities were observed for chlorinated solvents. Despite, the limited solubility we were able to record both ^{1}H and ^{13}C NMR in 1,1,2,2-tetrachloroethane-d_2. The ^{1}H NMR signals of cage **1** are broadened in comparison to those of the spectrum of the tetraldehyde precursor **2** (Fig. 2a). This broadening of the ^{1}H NMR signals is consistent with the limited solubility and signal splitting due to the presence of the chiral diaminocyclohexane residues. The observed broadening also indicates the formation of a conformationally-flexible structure, in agreement with previous reports on similar molecular cages.[37,38] The ^{1}H NMR spectrum of cage **1** at 25 °C shows a signal that correspond to the imine protons (a''), which is also observed on reference **4** (a'), and lacks the aldehyde protons signal (a) observed on spectrum of the tetraaldehyde precursor **2** (Fig. 2a), which confirms that all aldehydes have been transformed into imines. Moreover, the Fourier-transformed infrared (FT-IR) spectrum of cage **1** shows the imine C=N stretching signal at 1635 cm^{-1} (Fig. S1†), whereas the characteristic aldehyde C=O and C–H stretching observed in the spectrum of tetraldehyde **2** signals were not observed, which is also consistent with the transformation of all aldehydes into imines. We were unable to record a ^{1}H NMR spectrum at higher temperatures, as heating the sample in 1,1,2,2-tetrachloroethane resulted in the formation of a viscous material at 60 °C that we attributed to the partial hydrolysis and polymerization of the cage components in this solvent. This behavior is consistent with the limited stability of imine cages. To confirm that the broadening of the signals in the NMR

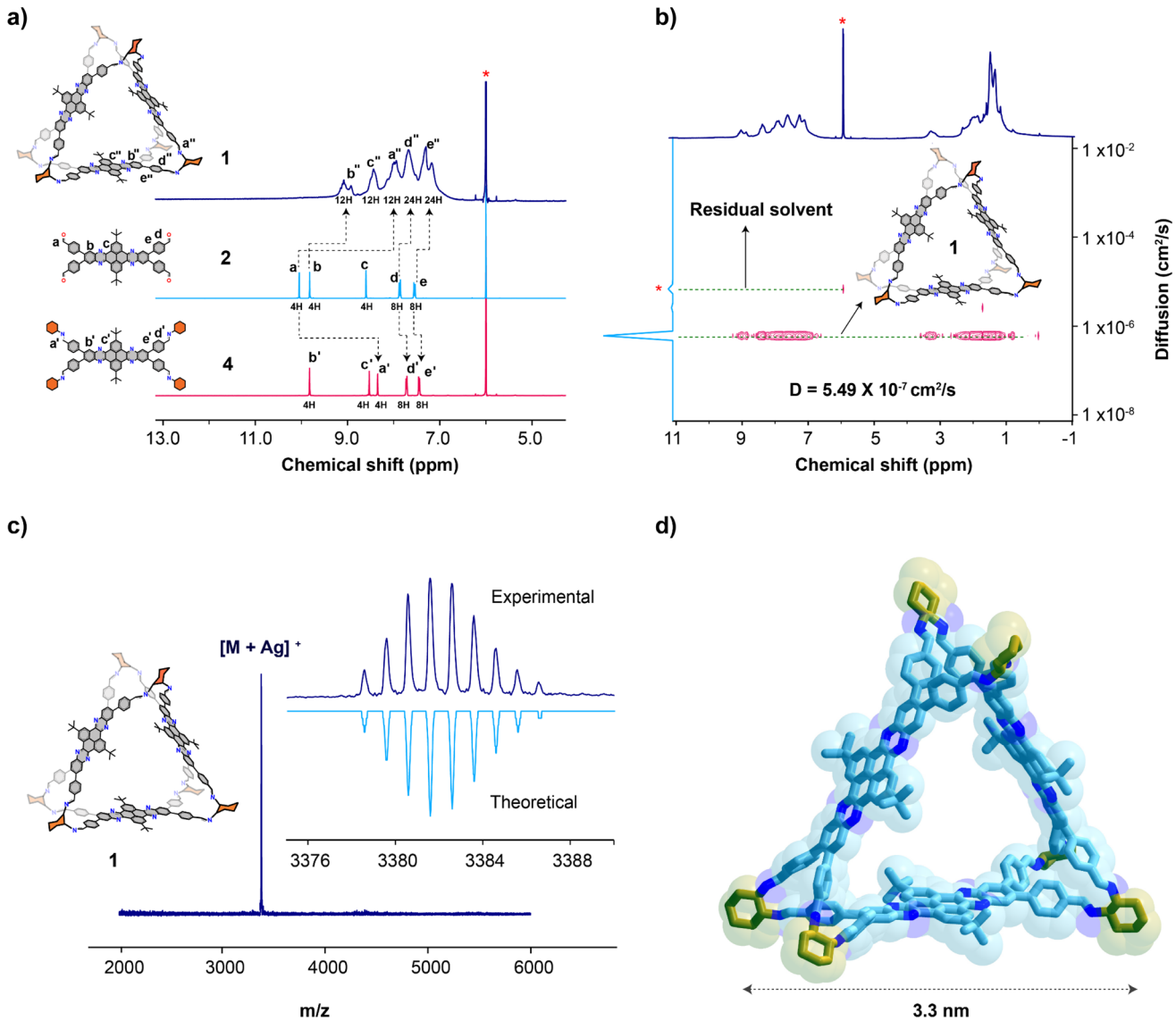

Fig. 2 (a) ^{1}H NMR spectra of cage **1**, tetraaldehyde **2** and reference **4** in 1,1,2,2-tetrachloroethane-d_2. (b) DOSY spectrum of cage **1** in 1,1,2,2-tetrachloroethane-d_2. Asterisk indicates solvent residual peaks. (c) Experimental (MALDI-TOF) and theoretical isotopic distributions of the [M + Ag]$^{+}$ ion peak of cage **1**. (d) Calculated structure of cage **1**.

spectrum of cage **1** is not due to the formation of cages with a different stoichiometry, a diffusion-ordered spectroscopy (DOSY) NMR spectrum was recorded (Fig. 2b). The DOSY spectrum of cage **1** shows how ^{1}H NMR signals diffuse at the same rate (5.5×10^{-7} cm^2 s^{-1}), demonstrating that all signals belong to a single cage species. Otherwise, if cages of different stoichiometries had been present, additional sets of signals diffusing at different rates would have been present. The ^{13}C NMR spectrum of cage **1** shows the same features observed by ^{1}H NMR, namely shifts consistent with the formation of the imine and signal broadening consistent with the low solubility and flexibility of the cage (Fig. S2†). The [3 + 6] stoichiometry of cage **1** was confirmed by matrix-assisted laser desorption ionization time-of-flight mass spectrometry (MALDI-TOF MS). The MS spectrum showed the $[M + Ag]^+$ molecular ion peak with an isotopic pattern consistent with the theoretical molecular weight and isotopic distribution of cage **1** (Fig. 2c). Furthermore, the peaks corresponding to cages with different stoichiometries, *e.g.* [2 + 4] or [4 + 8] species (Fig. S3†), were not detected, which is consistent with the findings observed in the DOSY spectrum of cage **1** that evidence the formation of a single stoichiometry cage product. The UV-vis and fluorescence spectra of cage **1** shows similar absorption and emission bands observed in tetraaldehyde **2** and reference **4** (Fig. S4†). Thermal gravimetric analysis (TGA) stability under nitrogen shows that cage **1** is thermally stable up to ~200 °C (Fig. S5†).

The molecular structure of **1** was constructed from an analogous cage molecule,[37] since all our attempts to grow crystals from the amorphous powders of cage **1** (Fig. S6†) were unsuccessful. In order to explore conformational space, a 2.5 ns molecular dynamics simulation was performed with the eXtended Tight Binding (xTB) methodology at 400 K in a solvent continuum.[39,40] From this, different conformations were selected, optimized and energy ranked at the xTB-GFN2 level first[41] to be further refined at the density functional theory (DFT) M06-2X-6-31G(d,p)-chloroform level yielding different conformers of which only one is populated at room temperature (Fig. 2d and S7†).[42,43] The energy optimized molecular structure of cage **1** shows a symmetrical triangular prismatic structure in which three dibenzotetraazahexacene panels are clipped through the imines of six diamine **3** units at the vertices. This arrangement generates two large triangular windows with a pore size of 1.37 nm (Fig. 2d) that should allow the diffusion of lithium cations (ionic diameter = 0.15 nm) across the cage.

The redox activity of cage **1** has been investigated by cyclic voltammetry in a three-electrode configuration using a traditional lithium-ion battery electrolyte (1 M $LiPF_6$ in ethylene carbonate and diethyl carbonate, 50/50 v/v) and compared to that of reference **4** (Fig. 3a and b). Both in the case of cage **1** and reference **4**, the reduction and oxidation peak potentials are anodically shifted upon cycling. The anodic shifts are consistent with the activation of the electrode after several cycles as previously described for electrodes constituted by covalent organic frameworks.[32] After this activation, two clear redox waves are observed at a formal potential of 3.00 and 2.84 V *vs.* Li/Li$^+$ in the case of cage **1**. These two processes are consistent with two sequential reductions of each quinoxaline group that generate first the diradical dianion and then the tetraanion (Fig. 3c and d), in analogy to other derivatives constituted by quinoxaline groups such as phenazine and hexaazatrinaphtylene derivatives[22,30–35] and with theoretical calculations (see below). Notably, no decay in the peak current of both the oxidation and reduction processes was observed for cage **1** upon cycling. Whereas, in the case of reference **4**, a significant decrease in peak current was observed for both oxidation and reduction peaks. In addition, while no colour change of the electrolyte solution was observed during the voltametric measurements on cage **1**, a clear colour change of the electrolyte solution, from transparent to yellow (same yellow colour as that of reference **4**), was observed during the measurements on reference **4**. This coloration indicates the leaching of reference **4** into the electrolyte, which compromises the long-term electrode stability. Whereas, the lack of coloration during the measurements on cage 1 illustrates the lower solubility of cage 1 and the enhanced electrode stability.

The mechanism set out in Fig. 3c was further supported by theoretical calculations (Fig. 3d). The frontier electronic levels of both molecules **4** and **1**, are very similar (Table S1 and Fig. S8†). The cage shows the expected three-fold degeneration with respect to **4** and, fundamentally, the same eigenvalues and the same HOMO–LUMO gaps. This is consistent with the fact that the dibenzotetraazahexacene units are electronically uncoupled to each other due to geometrical constraints and the lack of conjugation along the cyclohexanediimine linkers. In the case of the reference compound **4**, the electronic densities corresponding to the LUMO+1 and the LUMO at ~2.3 eV are located in the dibenzotetraazahexacene moieties, indicating that each of these moieties can accommodate up to four electrons. An analysis of the DFT-derived atomic charges in **1** and **4** reveals that the N_{sp_2} atoms in both molecules have similar charges around −0.36 and −0.33 for imine and pyrazinic N respectively, showing only very slight variations between both molecules (Fig. S9–S12†). These atoms function as electrostatic hotspots attracting Li$^+$ as the molecular electrostatic potential also shows, in line with previous reports.[22,31–35] To shine additional light, we systematically explored the Li$^+$ adsorption and reduction processes with extended tight-binding methodologies refined by *ab initio* DFT calculations (complete details can be found in the ESI†). This revealed that the most thermodynamically likely Li$^+$ adsorption sites are in the vicinity of pyrazinic N atoms during the two sequential two-electron reductions, with potentials of 2.79 and 2.63 V (Fig. S13†) that are consistent with those of the experimental measurements.

To further understand the impact of the cage architecture on the lithium transport properties, lithium-ion diffusion coefficients (D_{Li^+}) of cage **1** and of reference **4** were estimated by electrochemical impedance spectroscopy (Fig. 3e and S14†). Cage **1** exhibits a higher D_{Li^+} than that of reference **4** (5.25×10^{-10} and 9.03×10^{-11} cm^2 s^{-1}, respectively). This is consistent with the presence of large windows in cage **1** that favour the diffusion of lithium ions, as in the case of macrocyclic materials[44] and covalent organic frameworks.[45]

To have an additional insight the electrochemical performance of cage **1**, a cathode was formulated using cage **1** as the

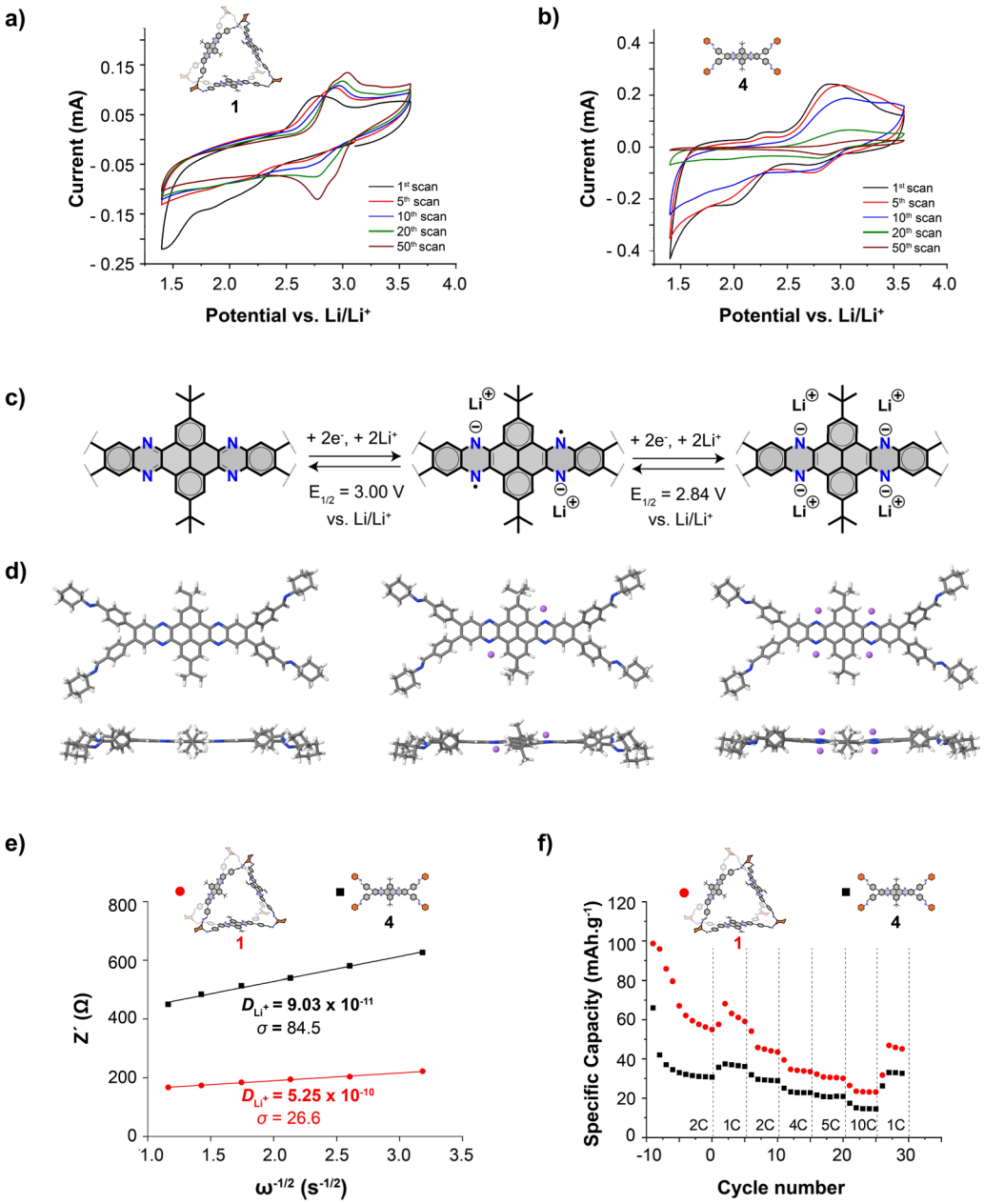

Fig. 3 Cyclic voltammograms of (a) cage **1** and (b) reference **4** in 1 M $LiPF_6$ in EC/DEC at a scan rate of 50 mV s^{-1}. Only 1st (black), 5th (red), 10th (blue), 20th (green) and 50th (brown) scans are shown for clarity. (c) Schematic representation of the redox processes in cage **1** and reference **4**. (d) Reduced states of **4** screened with DFT, top and side views (e) Z' (real part of impedance) *vs.* inverse square root of angular speed ($\omega^{-1/2}$) at low-frequency regime of electrochemical impedance spectra. The Warburg factor (σ) was obtained from the slope to calculate the diffusion coefficient for both the cage **1** (red) and reference molecule **4** (black). (f) Rate capability of a Li|**1** cell (red) and a Li|**4** cell (black) when cycled a various C-rate, ranging from 1C to 10C. Specific capacity as a function of cycle number.

active material, Super C65 and styrene-ethylene/butylene-styrene as conductive carbon and binder (20 : 70 : 10 wt%, respectively) and its cycling performance was investigated in a lithium metal battery at various C-rate (Fig. S15 and S16†). C-rate is defined as the rate of time required to fully charge or discharge a battery, based on the theoretical capacity of the electroactive material used in the electrode and can be defined as follows:

$$\text{C-rate} = i_{\text{applied}}/i_{1\text{h}}$$

where $i_{1\text{h}}$ is the current (A) required to fully oxidize or reduce an electroactive material in 1 hour. First, the Li|cage **1** cell was conditioned for 10 cycles at a C-rate of 2C prior assessing its performance at C-rates from 1C to 10C, due to the activation phenomenon observed in the cyclic voltammetry. At 1C, the Li|cage **1** cell exhibited two clear charge and discharge plateau at a voltage of around 3.2 V and 2.0 V *vs.* Li/Li^+. These voltages

are slightly offset when compared to the ones obtained from cyclic voltammetry, likely due to the higher loading of active material in the electrode used in the lithium metal cell, which would result in an increase of resistance and thus a slight shift in the voltage of the (dis-) charge plateau. The Li|cage **1** cell delivered a specific discharge capacity of 68 mA h g^{-1} (normalized by gram of cage **1**), which corresponds to 70% of its theoretical capacity of 98 mA h g^{-1} (Fig. S15†). Although a slight fading in terms of the capacity was observed upon the first five cycle at 1C, no significant capacity fading is observed upon increasing C-rate. The Li|cage **1** cell exhibited good rate capability, with a capacity retention of 39% at a C-rate of 10C when compared to 1C. Additionally, a more stable specific discharge of 47 mA h g^{-1} was obtained when cycling back to 1C (Fig. S16†). Most importantly, the Li|reference **4** cell shows a lower capacity at all the C-rate when compared with the Li|cage **1** cell (Fig. 3f). The enhanced rate capability of the cage **1** is in agreement with the superior lithium-ion transport property of cage **1**, highlighted by the lithium-ion diffusion coefficient measurements. Long-term cycling stability of the cage **1** was also investigated at a selected C-rate of 4C (Fig. S17†). A specific discharge capacity of 83 mA h g^{-1} was initially reached, which rapidly faded to 51 mA h g^{-1} in the first three cycles. Upon further cycling, a more moderate fading was observed with a remaining specific discharge capacity of 28 mA h g^{-1} after 100 cycles, suggesting that some degradation is occurring. Long-term cycling of Li|cage **1** cell was also investigated at a much higher C-rate (10C). Similarly, a rapid capacity fading was observed in the first three cycles, however a more stable cycling stability is observed upon further cycling, with a remaining specific discharge capacity of 28 mA h g^{-1} after 100 cycles (Fig. S18†).

Conclusions

In summary, we have shown how the incorporation of redox subunits into a cage-like structure leads to organic cathodes with enhanced performance when compared with cathodes fabricated from the individual subunits. This enhancement manifests in terms of cycling stability, lithium-ion diffusivity, and cathode capacity. The improvement in performance is consistent with the reduced solubility of the cage, which prevents leaching into the electrolyte, and with the presence of large windows that favour the diffusion of lithium ions. Overall, this work opens new possibilities for OCs and also for the design and development of new organic electrode materials with enhanced performance for energy applications, in which cage stoichiometry might play an active role.

Data availability

The data supporting this article have been included as part of the ESI.†

Author contributions

S. B. carried out the synthesis and characterization of the cages. N. G. fabricated and characterized the electrodes. M. M.-F. carried out the theoretical work. A. M.-A. and D. M. conceptualized and supervised the project. All authors further contributed to the discussion of the experimental work and the final version of the manuscript.

Conflicts of interest

There are no conflicts to declare.

Acknowledgements

This work was carried out with support from the Basque Science Foundation for Science (Ikerbasque), POLYMAT, the University of the Basque Country, Diputación de Guipúzcoa, Gobierno Vasco (PIBA and BERC programme) and Gobierno de España (Projects PID2021-124484OB-I00 and CEX2020-001067-M financed by MCIN/AEI/10.13039/501100011033). This project has received funding from the European Research Council (ERC) under the European Union's Horizon 2020 Research and Innovation Programme (Grant Agreement No. 722951). This work was funded by the European Union under the Horizon Europe grant 101046231. Project (PCI2022-132921) funded by the Agencia Estatal de Investigación through the PCI 2022 and M-ERA.NET 2021 calls. Technical and human support provided by SGIker of UPV/EHU and European funding (ERDF and ESF) is acknowledged. Support within the scope of the project CICECO-Aveiro Institute of Materials, UIDB/50011/2020 (**https://doi.org/10.54499/UIDB/50011/2020**), UIDP/50011/2020 (**https://doi.org/10.54499/UIDP/50011/2020**) and LA/P/0006/2020 (**https://doi.org/10.54499/LA/P/0006/2020**), financed by national funds through the FCT/MCTES (PIDDAC) is gratefully acknowledged. N. Goujon acknowledges the funding from the European Union's Horizon 2020 framework programme under the Marie Skłodowska-Curie agreement No. 101028682.

Notes and references

1 X. Yang, Z. Ullah, J. F. Stoddart and C. T. Yavuz, Porous Organic Cages, *Chem. Rev.*, 2023, **123**, 4602–4634.
2 G. Montà-González, F. Sancenón, R. Martínez-Máñez and V. Martí-Centelles, Purely Covalent Molecular Cages and Containers for Guest Encapsulation, *Chem. Rev.*, 2022, **122**, 13636–13708.
3 G. Zhang and M. Mastalerz, Organic cage compounds – from shape-persistency to function, *Chem. Soc. Rev.*, 2014, **43**, 1934–1947.
4 F. Beuerle and B. Gole, Covalent Organic Frameworks and Cage Compounds: Design and Applications of Polymeric and Discrete Organic Scaffolds, *Angew. Chem., Int. Ed.*, 2018, **57**, 4850–4878.
5 T. Hasell and A. I. Cooper, Porous organic cages: soluble, modular and molecular pores, *Nat. Rev. Mater.*, 2016, **1**, 16053.
6 X. Yang, J.-K. Sun, M. Kitta, H. Pang and Q. Xu, Encapsulating highly catalytically active metal nanoclusters inside porous organic cages, *Nat. Catal.*, 2018, **1**, 214–220.

7 C. Zhang, Q. Wang, H. Long and W. Zhang, A Highly C70 Selective Shape-Persistent Rectangular Prism Constructed through One-Step Alkyne Metathesis, *J. Am. Chem. Soc.*, 2011, **133**, 20995–21001.

8 T. Hasell, M. Miklitz, A. Stephenson, M. A. Little, S. Y. Chong, R. Clowes, L. Chen, D. Holden, G. A. Tribello, K. E. Jelfs and A. I. Cooper, Porous Organic Cages for Sulfur Hexafluoride Separation, *J. Am. Chem. Soc.*, 2016, **138**, 1653–1659.

9 M. Liu, L. Zhang, M. A. Little, V. Kapil, M. Ceriotti, S. Yang, L. Ding, D. L. Holden, R. Balderas-Xicohténcatl, D. He, R. Clowes, S. Y. Chong, G. Schütz, L. Chen, M. Hirscher and A. I. Cooper, Barely porous organic cages for hydrogen isotope separation, *Science*, 2019, **366**, 613–620.

10 Q. Song, S. Jiang, T. Hasell, M. Liu, S. Sun, A. K. Cheetham, E. Sivaniah and A. I. Cooper, Porous Organic Cage Thin Films and Molecular-Sieving Membranes, *Adv. Mater.*, 2016, **28**, 2629–2637.

11 L. Chen, P. S. Reiss, S. Y. Chong, D. Holden, K. E. Jelfs, T. Hasell, M. A. Little, A. Kewley, M. E. Briggs, A. Stephenson, K. M. Thomas, J. A. Armstrong, J. Bell, J. Busto, R. Noel, J. Liu, D. M. Strachan, P. K. Thallapally and A. I. Cooper, Separation of rare gases and chiral molecules by selective binding in porous organic cages, *Nat. Mater.*, 2014, **13**, 954–960.

12 R. Saha, B. Mondal and P. S. Mukherjee, Molecular Cavity for Catalysis and Formation of Metal Nanoparticles for Use in Catalysis, *Chem. Rev.*, 2022, **122**, 12244–12307.

13 V. Leonhardt, S. Fimmel, A.-M. Krause and F. Beuerle, A covalent organic cage compound acting as a supramolecular shadow mask for the regioselective functionalization of C60, *Chem. Sci.*, 2020, **11**, 8409–8415.

14 T.-C. Lee, E. Kalenius, A. I. Lazar, K. I. Assaf, N. Kuhnert, C. H. Grün, J. Jänis, O. A. Scherman and W. M. Nau, Chemistry inside molecular containers in the gas phase, *Nat. Chem.*, 2013, **5**, 376–382.

15 N. Giri, M. G. Del Pópolo, G. Melaugh, R. L. Greenaway, K. Rätzke, T. Koschine, L. Pison, M. F. C. Gomes, A. I. Cooper and S. L. James, Liquids with permanent porosity, *Nature*, 2015, **527**, 216–220.

16 A. Petronico, T. P. Moneypenny II, B. G. Nicolau, J. S. Moore, R. G. Nuzzo and A. A. Gewirth, Solid–Liquid Lithium Electrolyte Nanocomposites Derived from Porous Molecular Cages, *J. Am. Chem. Soc.*, 2018, **140**, 7504–7509.

17 J. Li, J. Qi, F. Jin, F. Zhang, L. Zheng, L. Tang, R. Huang, J. Xu, H. Chen, M. Liu, Y. Qiu, A. I. Cooper, Y. Shen and L. Chen, Room temperature all-solid-state lithium batteries based on a soluble organic cage ionic conductor, *Nat. Commun.*, 2022, **13**, 2031.

18 X. Zhang, K. Su, A. G. A. Mohamed, C. Liu, Q. Sun, D. Yuan, Y. Wang, W. Xue and Y. Wang, Photo-assisted charge/discharge Li-organic battery with a charge-separated and redox-active C60@porous organic cage cathode, *Energy Environ. Sci.*, 2022, **15**, 780–785.

19 L. Zhang, Y. Jia, F. Meng, L. Sun, F. Cheng, Z. Shi, R. Jiang and X. Song, A naphthalene organic cage captured sodium polysulphide as cathode materials for lithium-ion sulfide batteries, *J. Alloys Compd.*, 2022, **923**, 166488.

20 H. Li, Y. Huang, Y. Zhang, X. Zhang, L. Zhao, W. Bao, X. Cai, K. Zhang, H. Zhao, B. Yi, L. Su, A. K. Cheetham, S. Jiang and J. Xie, An Ultrathin Functional Layer Based on Porous Organic Cages for Selective Ion Sieving and Lithium–Sulfur Batteries, *Nano Lett.*, 2022, **22**, 2030–2037.

21 Y. Xie, M. Yang, E.-S. M. El-Sayed, K. Su, Z. Li and D. Yuan, Porous Organic Cage as a Sulfur Host for Upgrading Capacity and Longevity of Li–S Batteries, *ACS Appl. Nano Mater.*, 2023, **6**, 7910–7919.

22 H. Dong, N. Kang, L. Li, L. Li, Y. Yu and S. Chou, Versatile Nitrogen-Centered Organic Redox-Active Materials for Alkali Metal-Ion Batteries, *Adv. Mater.*, 2024, 2311401.

23 N. Goujon, N. Casado, N. Patil, R. Marcilla and D. Mecerreyes, Organic batteries based on just redox polymers, *Prog. Polym. Sci.*, 2021, **122**, 101449.

24 X. Zhao, P. Pachfule and A. Thomas, Covalent organic frameworks (COFs) for electrochemical applications, *Chem. Soc. Rev.*, 2021, **50**, 6871–6913.

25 Y. Lu and J. Chen, Prospects of organic electrode materials for practical lithium batteries, *Nat. Rev. Chem.*, 2020, **4**, 127–142.

26 P. Poizot, J. Gaubicher, S. Renault, L. Dubois, Y. Liang and Y. Yao, Opportunities and Challenges for Organic Electrodes in Electrochemical Energy Storage, *Chem. Rev.*, 2020, **120**, 6490–6557.

27 J. Heiska, M. Nisula and M. Karppinen, Organic electrode materials with solid-state battery technology, *J. Mater. Chem. A*, 2019, **7**, 18735–18758.

28 M. E. Bhosale, S. Chae, J. M. Kim and J.-Y. Choi, Organic small molecules and polymers as an electrode material for rechargeable lithium ion batteries, *J. Mater. Chem. A*, 2018, **6**, 19885–19911.

29 Y. Zhang, J. Wang and S. N. Riduan, Strategies toward improving the performance of organic electrodes in rechargeable lithium (sodium) batteries, *J. Mater. Chem. A*, 2016, **4**, 14902–14914.

30 C. N. Gannett, B. M. Peterson, L. Shen, J. Seok, B. P. Fors and H. D. Abruña, Cross-linking Effects on Performance Metrics of Phenazine-Based Polymer Cathodes, *ChemSusChem*, 2020, **13**, 2428–2435.

31 C. de la Cruz, A. Molina, N. Patil, E. Ventosa, R. Marcilla and A. Mavrandonakis, New insights into phenazine-based organic redox flow batteries by using high-throughput DFT modelling, *Sustainable Energy & Fuels*, 2020, **4**, 5513–5521.

32 E. Vitaku, C. N. Gannett, K. L. Carpenter, L. Shen, H. D. Abruña and W. R. Dichtel, Phenazine-Based Covalent Organic Framework Cathode Materials with High Energy and Power Densities, *J. Am. Chem. Soc.*, 2020, **142**, 16–20.

33 C. Peng, G.-H. Ning, J. Su, G. Zhong, W. Tang, B. Tian, C. Su, D. Yu, L. Zu, J. Yang, M.-F. Ng, Y.-S. Hu, Y. Yang, M. Armand and K. P. Loh, Reversible multi-electron redox chemistry of π-conjugated N-containing heteroaromatic molecule-based organic cathodes, *Nat. Energy*, 2017, **2**, 17074.

34 F. Xu, X. Chen, Z. Tang, D. Wu, R. Fu and D. Jiang, Redox-active conjugated microporous polymers: a new organic platform for highly efficient energy storage, *Chem. Commun.*, 2014, **50**, 4788–4790.

35 Z. Sun, H. Liu, M. Shu, Z. Lin, B. Liu, Y. Li, J. Li, T. Yu, H. Yao, S. Zhu and S. Guan, π-Conjugated Hexaazatrinaphthylene-Based Azo Polymer Cathode Material Synthesized by a Reductive Homocoupling Reaction for Organic Lithium-Ion Batteries, *ACS Appl. Mater. Interfaces*, 2022, **14**, 36700–36710.

36 E. De Bolòs, M. Martínez-Abadía, F. Hernández-Culebras, A. Haymaker, K. Swain, K. Strutyński, B. L. Weare, J. Castells-Gil, N. M. Padial, C. Martí-Gastaldo, A. N. Khlobystov, A. Saeki, M. Melle-Franco, B. L. Nannenga and A. Mateo-Alonso, A Crystalline 1D Dynamic Covalent Polymer, *J. Am. Chem. Soc.*, 2022, **144**, 15443–15450.

37 S. Bera, S. Das, M. Melle-Franco and A. Mateo-Alonso, An Organic Molecular Nanobarrel that Hosts and Solubilizes C60, *Angew. Chem., Int. Ed.*, 2023, **62**, e202216540.

38 P. C. Purba, M. Maity, S. Bhattacharyya and P. S. Mukherjee, A Self-Assembled Palladium(II) Barrel for Binding of Fullerenes and Photosensitization Ability of the Fullerene-Encapsulated Barrel, *Angew. Chem., Int. Ed.*, 2021, **60**, 14109–14116.

39 S. Spicher and S. Grimme, Robust Atomistic Modeling of Materials, Organometallic, and Biochemical Systems, *Angew. Chem., Int. Ed.*, 2020, **59**, 15665–15673.

40 C. Bannwarth, E. Caldeweyher, S. Ehlert, A. Hansen, P. Pracht, J. Seibert, S. Spicher and S. Grimme, Extended tight-binding quantum chemistry methods, *Wiley Interdiscip. Rev.: Comput. Mol. Sci.*, 2021, **11**, e1493.

41 C. Bannwarth, S. Ehlert and S. Grimme, GFN2-xTB—An Accurate and Broadly Parametrized Self-Consistent Tight-Binding Quantum Chemical Method with Multipole Electrostatics and Density-Dependent Dispersion Contributions, *J. Chem. Theory Comput.*, 2019, **15**, 1652–1671.

42 P. Pracht, F. Bohle and S. Grimme, Automated exploration of the low-energy chemical space with fast quantum chemical methods, *Phys. Chem. Chem. Phys.*, 2020, **22**, 7169–7192.

43 M. J. Frisch, G. W. Trucks, H. B. Schlegel, G. E. Scuseria, M. A. Robb, J. R. Cheeseman, G. Scalmani, V. Barone, G. A. Petersson, H. Nakatsuji, X. Li, M. Caricato, A. V. Marenich, J. Bloino, B. G. Janesko, R. Gomperts, B. Mennucci, H. P. Hratchian, J. V. Ortiz, A. F. Izmaylov, J. L. Sonnenberg, D. Williams-Young, F. Ding, F. Lipparini, F. Egidi, J. Goings, B. Peng, A. Petrone, T. Henderson, D. Ranasinghe, V. G. Zakrzewski, J. Gao, N. Rega, G. Zheng, W. Liang, M. Hada, M. Ehara, K. Toyota, R. Fukuda, J. Hasegawa, M. Ishida, T. Nakajima, Y. Honda, O. Kitao, H. Nakai, T. Vreven, K. Throssell, J. A. Montgomery Jr, J. E. Peralta, F. Ogliaro, M. J. Bearpark, J. J. Heyd, E. N. Brothers, K. N. Kudin, V. N. Staroverov, T. A. Keith, R. Kobayashi, J. Normand, K. Raghavachari, A. P. Rendell, J. C. Burant, S. S. Iyengar, J. Tomasi, M. Cossi, J. M. Millam, M. Klene, C. Adamo, R. Cammi, J. W. Ochterski, R. L. Martin, K. Morokuma, O. Farkas, J. B. Foresman and D. J. Fox, *Gaussian 16 Rev. C.01*, Wallingford, CT, 2016.

44 D. Chen, A.-J. Avestro, Z. Chen, J. Sun, S. Wang, M. Xiao, Z. Erno, M. M. Algaradah, M. S. Nassar, K. Amine, Y. Meng and J. F. Stoddart, A Rigid Naphthalenediimide Triangle for Organic Rechargeable Lithium-Ion Batteries, *Adv. Mater.*, 2015, **27**, 2907–2912.

45 Z. Luo, L. Liu, J. Ning, K. Lei, Y. Lu, F. Li and J. Chen, A Microporous Covalent–Organic Framework with Abundant Accessible Carbonyl Groups for Lithium-Ion Batteries, *Angew. Chem., Int. Ed.*, 2018, **57**, 9443–9446.